Frontiers in Life Sciences and Related Technologies 4(3) (2023) 138-144

Contents lists available at Dergipark

Frontiers in Life Sciences and Related Technologies

Journal homepage: http://dergipark.org.tr/en/pub/flsrt

Research article

Comparison of the effects of different local thresholding techniques on noise: A potential for optical coherence tomography image binarization

Onur Inam*[1, 2]

[1] *Gazi University, Faculty of Medicine, Department of Biophysics, 06500, Ankara, Türkiye*
[2] *Columbia University, Edward S. Harkness Eye Institute, Vagelos College of Physicians and Surgeons, Columbia University Irving Medical Center, Department of Ophthalmology, 10032, New York, NY, USA*

Abstract

This study aims to investigate the different local thresholding methods on various regions of noise images, which could be used for image binarization of optical coherence tomography images. In the methods one hundred 8-bit images of noise, 1000x1000 pixel in size, is generated using ImageJ/FIJI program. Images processed with four different auto local threshold method in ImageJ/FIJI program as Niblack, mean, median and midgrey, to perform binarization. Twenty-five different region of interest, 100x100 pixel in size, from different region in an image analyzed for area percentage (AP) measurement. Normality tests were performed via Saphiro Wilk Normality test, and Student's t test and one-way ANOVA were used to assess the continuous variables, and Bonferroni test for post hoc analysis, utilizing the IBM SPSS Statistics for the statistical analysis. In the results of this study mean AP for Niblack method was 42.08 ± 0.32%, for mean method was 50.00 ± 0.32%, for median method was 49.28 ± 0.16%, and for midgrey method was 49.63 ± 2.09%. One-way ANOVA analysis shows all the different subgroups of Niblack and mean, Niblack and median, Niblack and midgrey, mean and median, mean and midgrey, and median and midgrey measurements are significantly different from each other. In conclusion this study examined 100 noise images across 25 regions using four auto local threshold methods (Niblack, mean, median, and midgrey). Analyses indicated that Niblack having the lowest mean and there is significant difference between all the methods; researchers using auto local threshold methods in OCT image processing should select methods aligned with data properties, warranting further exploration of these methods' impact on diverse OCT image, especially taking into account the effect of the noise.

Keywords: *Biophysics; choroidal vascularity index; image processing; optical coherence tomography; thresholding*

1. Introduction

Image processing in the ophthalmological instruments have long been an important issue since first optical coherence tomography (OCT) has been introduced. In this very first explanation of advantages of the device itself, researchers discussed and emphasized the non-invasive nature of the technique for biological systems (Huang et al., 1991). Since then it is widely used for various kind of ophthalmological conditions including retinal and choroidal pathologies, acquired and inherited conditions (Adhi and Duker, 2013).

The basics of the device rely on low coherence interferometry, a concept similar to ultrasonic pulse-echo imaging. However, the key distinction is that it employs near-infrared light (NIR) instead of sound waves. The formation and visualization of images occur through the measurement of both the time and magnitude delay of the light that is scattered back from the retina. Due to the rapid velocity of the light beams, direct echoes cannot be detected directly and to overcome this, a reference mirror is employed which facilitates the comparison

* Corresponding author.
E-mail address: onurinam@gazi.edu.tr (O. Inam).
https://doi.org/10.51753/flsrt.1350211 Author contributions
Received 27 August 2023; Accepted 12 October 2023
Available online 29 October 2023

of reflections using a Michelson interferometer (Huang et al., 1991).

Recent improvements in the OCT technology allowed us to use spectral domain OCT (SD-OCT), as a high-resolution diagnostic tool (Nassif et al., 2004). High-resolution means more data to interpret and more need for the analysis the data of the image has itself. Thus, OCT and various ophthalmological images become a natural candidate for the various kind of image processing approaches (Agrawal et al., 2016a,c).

Empowering as a few micrometers of resolution to the ophthalmological images, nearly as a histological image section, new OCT technologies are even a better target for many of the image processing methods (Sull et al., 2010). Optical coherence tomography angiography (OCT-A) technology further improved our understanding of functional and anatomical vessel interactions and properties (Ferrara et al., 2016; Kashani et al., 2017). OCT-A technology has a complex computational background which mainly utilizes the signal based approaches (Kashani et al., 2017).

Many of the studies that utilize from OCT, measures mainly the thickness of the retina and choroid (Leitgeb et al., 2003; Spaide et al., 2008; Adhi and Duker, 2013). These thickness measurements were performed in different regions of the ocular structures (Manjunath et al., 2010). The image processing of the OCT images is not limited to the thickness measurement. The studies for retinal image analysis ranges from image enhancement, segmentation to the thresholding. Not only OCT images of the macula and fovea have been a subject for image processing approaches, but also other anatomical structures like vessels, optic nerve and other structures have been important for the ophthalmological image processing studies. Even there were different imaging modalities except OCT (Patton et al., 2006).

In the recent years, a new field closely related to the image processing gain importance which is artificial intelligence. Many of the artificial intelligence study techniques have been studied in both anterior and posterior segment analysis. Thus, there are numerous parameters and indexes that can be used in artificial intelligence architectures, in order to diagnose and follow up distinct diseases (Duan et al., 2022; Gozzi et al., 2023). Moreover, some of these studies showed that artificial intelligence may help the clinician in the process of deciding to the surgery (Gan et al., 2022). Artificial intelligence is studied for its role in screening of some ophthalmological conditions, and found to be a valuable and promising tool (Huang et al., 2022).

One of the most studied areas of image analysis research is choroidal vascularity index (CVI) (Agrawal et al., 2016a,c). Previous image processing studies paved the road for CVI calculations (Sonoda et al., 2014). It mainly questions if the thickness measurements are not sufficient for further evaluation of many diseases, whether ophthalmological and non-ophthalmological ones such as from Stargardt disease to panuveitis and from Vogt-Koyanagi-Harada disease to type-2 diabetes (Agrawal et al., 2016b,c; Kim et al., 2018; Ratra et al., 2018). In this particular method, CVI is measured with a Niblack binarization technique in OCT images (Agrawal et al., 2016a,c).

Image processing studies utilizing CVI as a tool has a broad spectrum of interest. Using image processing methods, particularly CVI, different regions of the retina has been investigated like macula and peripapillary region (Qi et al., 2023). Also, there are studies that investigate drug effects, like hydroxychloroquine, and these kind of image analysis tools are mentioned to be a candidate tool for decision making (Hasan et al., 2023). One other study found that primary open-angle glaucoma and primary angle-closure glaucoma had significantly different CVI values (Wang et al., 2023).

Although OCT is an advantageous method for many reasons, the noise is a concern while gathering the images and there were certain approaches to overcome this situation in the literature, even using artificial intelligence (Qiu et al., 2020). Deep learning approaches also used to denoise the OCT images of the different ocular anatomical regions (Devalla et al., 2019). Thus, because of the nature of the Niblack binarization method, noise could be very important, for the interpretation of the outcome results.

The need for the determining basic characteristics of widely used Niblack method and other methods in noisy images, simulating the noisy part of the OCT images, is increasing as the CVI research gain importance. Use of different thresholding methods in different image conditions can be used as the purpose of the study. For this purpose, in this study it is aimed to investigate the role of Niblack and three other methods on noise images, in 25 different regions of the noise images.

2. Materials and methods

2.1. Image acquisition

One hundred different noise image is generated in Tiff format with a frame of 1000x1000 pixel, a square shaped image, using ImageJ/FIJI program (version 1.52b) (Schindelin et al., 2012; Schneider et al., 2012). These images were in 8-bit gray scale as in the most binarization techniques have been performed previously (Agrawal et al., 2016c) (Fig. 1A).

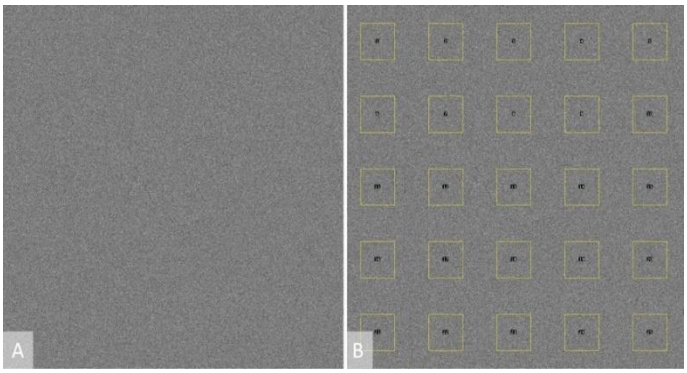

Fig. 1. (A) A sample noise image, (B) 25 Region of interest (ROI) that are measured in a single image.

2.2. Binarization process

Gray scale noise images have been employed in order to binarize via auto local threshold approaches. Binarization means rescaling two-digit value pixels, either 1 or 0, or simply white and black. Different techniques of local threshold methods for binarization are used as Niblack, mean, median and midgrey as in the previous studies (Fig. 2A-D, respectively). Auto local threshold is a plugin in the ImageJ/FIJI program, that are used to binarize images, which computes the threshold using different approaches such as Niblack, mean, median and midgrey as preset inbuilt methods (Agrawal et al., 2016c; Landini et al., 2017; Healy et al., 2018; Nichele et al., 2020).

2.3. Region of interests

After binarization of the image with a technique, new image has been saved and ROI measurements take place. Twenty-five independent regions of interest (ROI) drawn as shown in the Fig. 1B., in order to represent more of the noise area and randomize it. Dimension of the ROIs are 100x100 pixel square, 100 pixels apart each other, in an orientation of five horizontal and five vertical landing, a total of 25 per image. Thus, 25 different ROI for 100 image makes a total of 2500 ROI, which have been analyzed for binarization results with four different techniques.

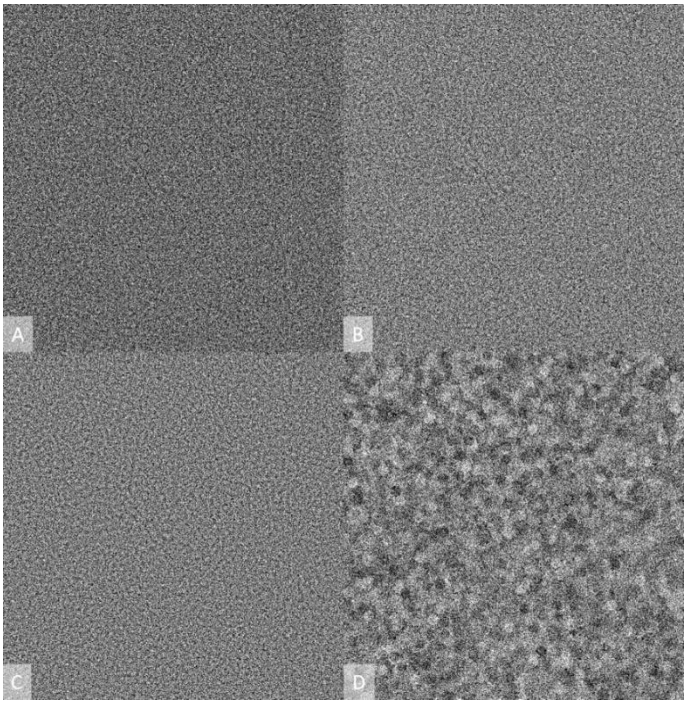

Fig. 2. (A) Binarized image using Niblack method, (B) Binarized image using mean method, (C) Binarized image using median method, (D) Binarized image using midgrey method.

2.4. Area percentage measurement

ROIs have been measured using measure function in the ROI manager tab of the program. In this section area percentage (AP) and mean pixel values were noted, and each ROI is investigated for the area fraction of white to the total area and showed in percentage. Histograms, boxplots and scatter plots of different methods have been drawn.

2.5. Statistical analysis

A total of 100 images with 25 different ROIs have been analyzed with four different auto local threshold technique. IBM SPSS Statistics, Version 28.0 is used for the statistical analysis. Techniques are compared between each other and for different regions with Student's T-test. One-way ANOVA has been employed for independent group assessment and Bonferroni post hoc analysis has been performed for further analysis. Normality tests were performed with Saphiro Wilk Normality tests. Continuous variables have been shown as mean and standard deviation. p value smaller than the 0.05 is accepted as significant.

3. Results and discussion

When the total measurements of all techniques analyzed, mean AP was measured as 47.75 ± 3.45% (41.11 - 55.84%, N = 10000). Mean AP for Niblack method was 42.08 ± 0.32% (41.11 - 43.21 %, N = 2500), for mean method was 50.00 ± 0.32% (49.02 - 51.28%, N = 2500) and for median method was 49.28 ± 0.16% (48.77 - 49.84%, N = 2500), for midgrey method was 49.63 ± 2.09% (42.34 - 55.84%, N = 2500) (Fig. 3).

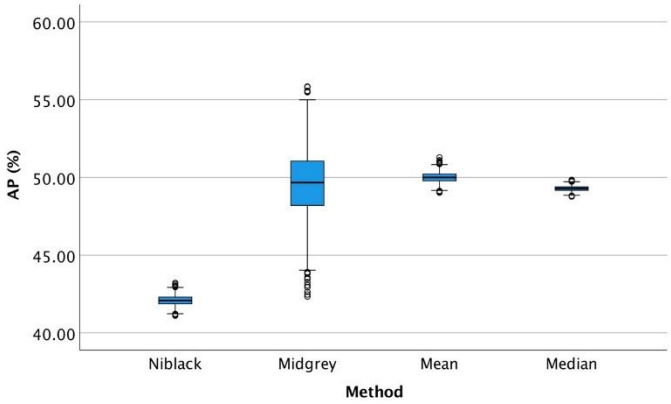

Fig. 3. Boxplot graphs of the four different auto local threshold methods: Niblack, midgrey, mean and median (AP: Area Percentage, %: Percent).

When Niblack and midgrey AP compared with each other, Niblack was found significantly lower than the midgrey (p< 0.001). The distribution width of midgrey, thus standard deviation is higher than the Niblack method, which can be seen in the Fig. 3 and Fig. 4. Niblack AP is significantly lower compared to both mean and median method APs (p<0.001 and p<0.001, respectively) (Fig. 3). AP of the midgrey is significantly lower than the mean and significantly higher than the median method (p<0.001 and p<0.001, respectively) (Fig. 3). And mean methods AP values are significantly higher than the median method (p<0.001) (Fig. 3). Although there is not a high difference between AP results, the high number of sampling rate makes small changes more significant. All the four methods results are normally distributed which can be seen at Fig. 4.

One-way ANOVA analysis showed that there were significant differences between 4 methods (p<0.001). Bonferroni post hoc analysis suggested that these differences were due to all of the sub groups of Niblack and mean, Niblack and median, Niblack and midgrey, mean and median, mean and midgrey, and median and midgrey (p<0.001 for all of the subgroup post hoc analysis).

Table 1
Mean values in different methods.

Method	Mean Pixel Value $\bar{x}\pm\sigma$	Minimum Pixel Value	Maximum Pixel Value
Niblack (n=2500)	107.31 ± 0.82	104.83	110.19
Mean (n=2500)	127.49 ± 0.82	125.00	130.76
Median (n=2500)	125.67 ± 0.41	124.36	127.09
Midgrey (n=2500)	126.55 ± 5.33	107.97	142.39

(n=Number, $\bar{x}$:Mean, σ:Standard Deviation)

Mean pixel value after binarization of different methods have been shown in the Table 1 which is typically between 0-255 in 8-bit images. The mean value of the Niblack method was

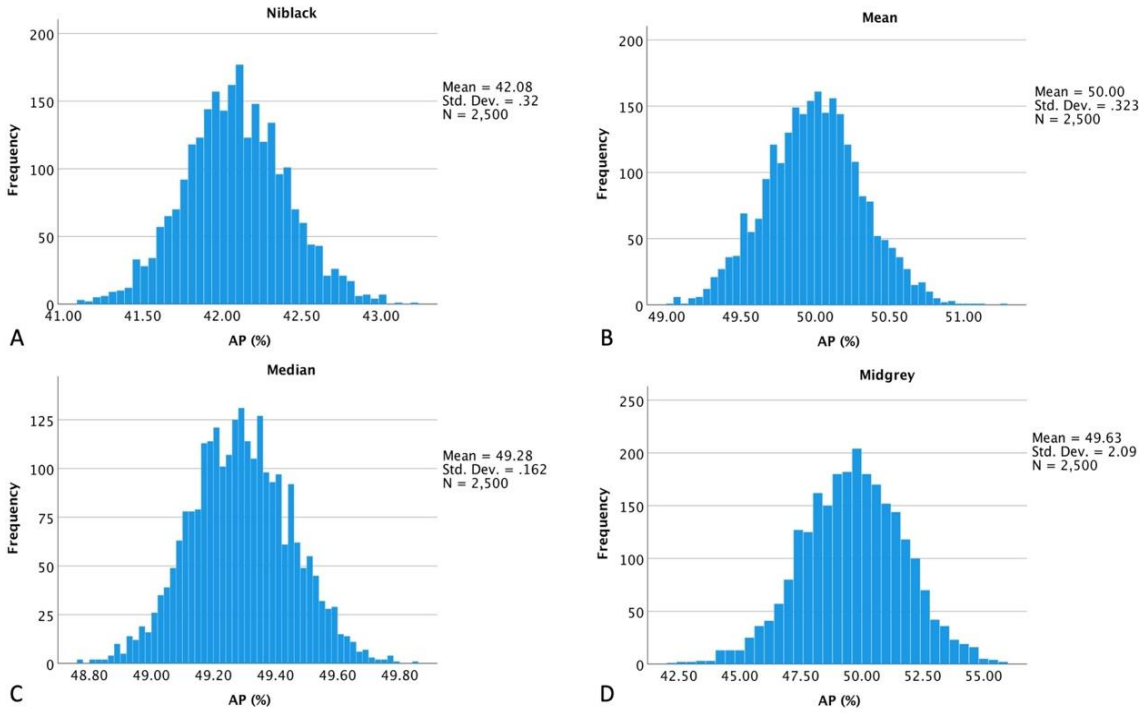

Fig. 4. Histogram graphs of the four different auto local threshold methods: (A) Niblack, (B) Mean, (C) Median, (D) Midgrey (AP: Area Percentage, %: Percent, Std. Dev.: Standard Deviation, N: Number).

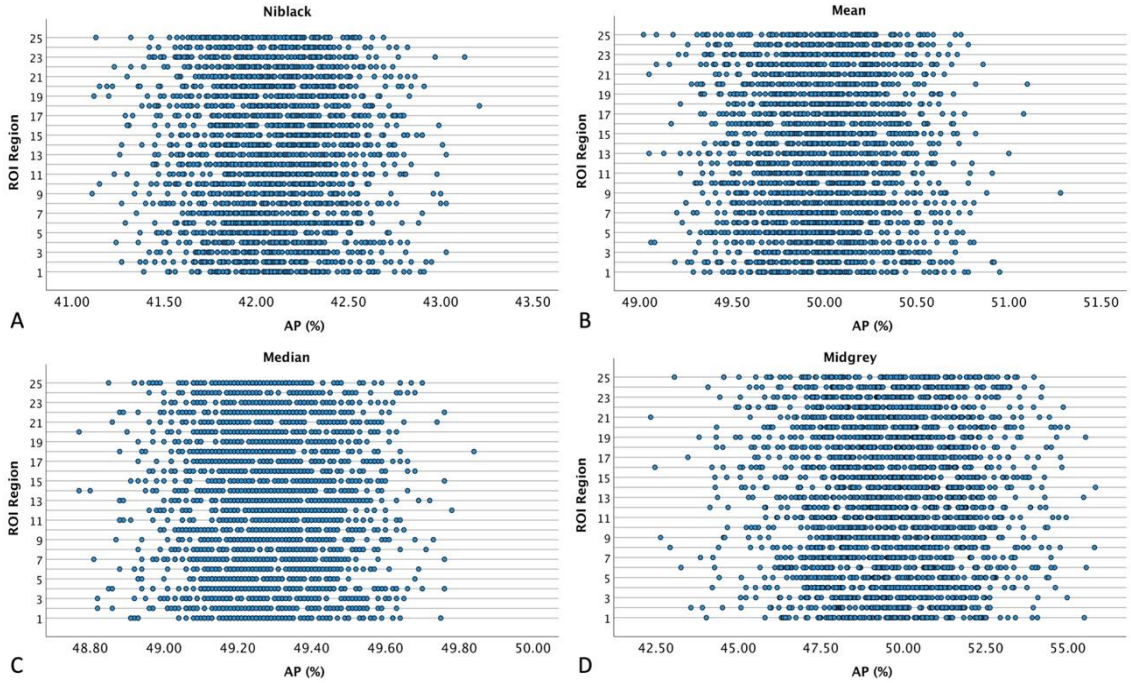

Fig. 5. Scatter plot graphs of the 25 different regions of the four different auto local threshold methods: (A) Niblack, (B) Mean, (C) Median, (D) Midgrey (AP: Area Percentage, %: Percent, ROI: Region of Interest).

found to be lowest among four different method, and mean method found to be highest (107.31 ± 0.82, 127.49 ± 0.82, respectively) (Table 1).

Scatter plot and box plot graphs showed that there are some outliers in all of the methods in different regions, which can be seen in Fig. 5 and Fig. 6.

These adaptive and local thresholding techniques have been used in a broad spectrum of images and studies including the CVI studies (Brocher, 2014; Agrawal et al., 2016a; Mohamed Razali et al., 2017; Healy et al., 2018; Nichele et al., 2020; Ban and Kweon, 2021). In a study investigating the adaptive thresholding methods in dental X-ray images, researchers compared the mean, median, midgrey, Otsu and Niblack methods and they have found that median method has the best thresholding range overall (Mohamed Razali et al., 2017). Another study in the literature mentioned the role of these methods in quantification of sweat areas in a mouse model (Ban and Kweon, 2021). Yet a study implies and investigates the role of these different methods on both experimental and synthetic confocal images of different bacteria types (Nichele et al., 2020).

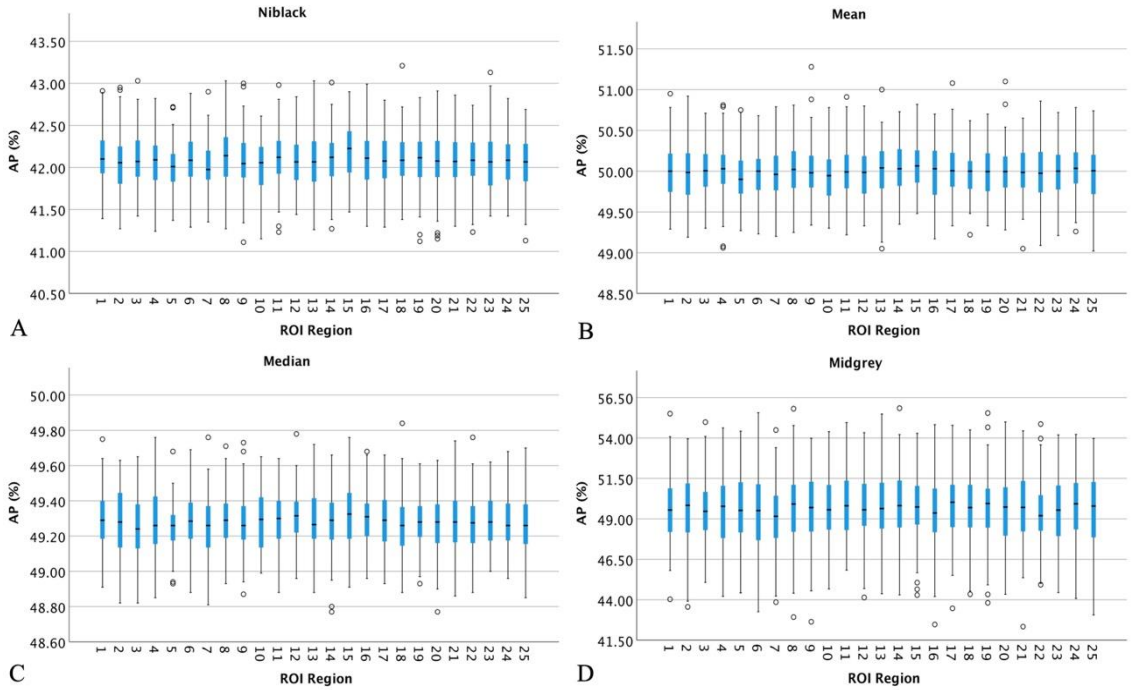

Fig. 6. Boxplot graphs of the 25 different regions of the four different auto local threshold methods: (A) Niblack, (B) Mean, (C) Median, (D) Midgrey (AP: Area Percentage, %: Percent, ROI: Region of Interest).

Different kind of images of astrocytes, microglia and oligodendrocytes were also evaluated using different thresholding methods including mean, median, midgrey, and Niblack (Healy et al., 2018). There were studies comparing new algorithms with pre-existing thresholding methods (Brocher, 2014).

Niblack method can be considered as a local thresholding method alongside many others like Sauvola (Niblack, 1986; Sauvola and Pietikäinen, 2000; Healy et al., 2018). Because Niblack method depends vastly on the mean and standard deviation in a local region around a particular pixel, the main aim of this method could be interpreted as making the thresholding process which takes into account that surrounding pixels; Thus, use of Niblack method could have both some advantages and disadvantages (Adeyanju et al., 2021).

In this study it is found that different adaptive thresholding methods has significantly different outcomes in the noise. Thus, especially images that has too much noise in it, can be vulnerable for that kind of different results when performed with different methods. Researchers should be careful about the methodology they chose, before they begin the study, depending on their dataset and the noise that contains. OCT images, especially that performed with an unsatisfied quality, should be considered for noise, if they will be included in studies that require for implementation of Niblack thresholding algorithm like CVI. There are some methods used for reducing the noise by reducing brightness of the OCT images, in order to get better results in the CVI assessment (Agrawal et al., 2016c). While the contrast disperse is uniform, global thresholding methods have advantages, whereas if the contrast is variable or noise is present, local thresholding methods gain importance (Singh and Mridula, 2014).

In this study it is performed analysis in different regions in a 1000x1000 pixel image with a ROI size of 100x100. A study in the literature performed a comparative analysis between different methods in confocal microscopic and synthetic images found that local thresholding techniques are very sensitive to the ROI size (Nichele et al., 2020). Thus, researchers should also consider the ROI size, when conducting a proper study that investigates utilizing local thresholding methods.

Considering its widespread investigation in recent years, CVI is a major research topic not only in medical but also in surgical and postsurgical conditions (Quiroz-Reyes et al., 2023). There are both advantages and disadvantages, strength and limitations of different thresholding algorithms (Nichele et al., 2020). Although CVI studies performed on the OCT images found Niblack method more reliable for showing luminal and stromal areas, other studies examining the dental X-ray images found median method more suitable for higher number of teeth segmentation (Agrawal et al., 2016c; Mohamed Razali et al., 2017).

Researchers should decide the correct thresholding method, for their study, considering the amount of noise in their datasets. This study sheds light on the basic characteristics in the noise images of various auto local thresholding methods.

4. Conclusion

In this study 100 noise images were investigated for 25 different regions and four different auto local threshold methods as Niblack, mean, median and midgrey. The findings indicated that the AP for all four methods followed a normal distribution. Additionally, there was a significant difference observed among subgroups, with the Niblack method exhibiting the lowest mean value. Although OCT is an advantageous imaging tool widely used in ophthalmology, noise in the OCT images could be a major problem, and researchers conduct image processing studies employing auto local threshold methods should consider their methods according to the properties of their data that they will work on. Future studies are needed for investigating the effects of different auto local thresholding methods during noise in various kind of OCT images.

Conflict of interest: The author declares that he has no conflict of interests.

Informed consent: The author declares that this manuscript did not involve human or animal participants and informed consent was not collected.

References

Adeyanju, I. A., Bello, O. O., & Adegboye, M. A. (2021). Machine learning methods for sign language recognition: A critical review and analysis. *Intelligent Systems with Applications*, *12*, 200056.

Adhi, M., & Duker, J. S. (2013). Optical coherence tomography--current and future applications. *Current Opinion in Ophthalmology*, *24*(3), 213-221.

Agrawal, R., Gupta, P., Tan, K. A., Cheung, C. M., Wong, T. Y., & Cheng, C. Y. (2016a). Choroidal vascularity index as a measure of vascular status of the choroid: Measurements in healthy eyes from a population-based study. *Scientific Reports*, *6*, 21090.

Agrawal, R., Li, L. K., Nakhate, V., Khandelwal, N., & Mahendradas, P. (2016b). Choroidal Vascularity Index in Vogt-Koyanagi-Harada Disease: An EDI-OCT Derived Tool for Monitoring Disease Progression. *Translational Vision Science & Technology*, *5*(4), 7.

Agrawal, R., Salman, M., Tan, K. A., Karampelas, M., Sim, D. A., Keane, P. A., & Pavesio, C. (2016c). Choroidal vascularity index (CVI)--A novel optical coherence tomography parameter for monitoring patients with panuveitis? *PLoS One*, *11*(1), e0146344.

Ban, C., & Kweon, D.-H. (2021). Objective Quantitation of Focal Sweating Areas Using a Mouse Sweat-assay Model. *Bio-protocol*, *11*(11), e4047.

Brocher, J. (2014). Qualitative and quantitative evaluation of two new histogram limiting binarization algorithms. *International Journal of Image Processing*, *8*(2), 30-48.

Devalla, S. K., Subramanian, G., Pham, T. H., Wang, X., Perera, S., Tun, T. A., ... & Girard, M. J. (2019). A deep learning approach to denoise optical coherence tomography images of the optic nerve head. *Scientific Reports*, *9*(1), 14454.

Duan, S., Huang, P., Chen, M., Wang, T., Sun, X., Chen, M., Dong, X., Jiang, Z., & Li, D. (2022). Semi-supervised classification of fundus images combined with CNN and GCN. *Journal of Applied Clinical Medical Physics*, *23*(12), e13746.

Ferrara, D., Waheed, N. K., & Duker, J. S. (2016). Investigating the choriocapillaris and choroidal vasculature with new optical coherence tomography technologies. *Progress in Retinal and Eye Research*, *52*, 130-155.

Gan, F., Chen, W. Y., Liu, H., & Zhong, Y. L. (2022). Application of artificial intelligence models for detecting the pterygium that requires surgical treatment based on anterior segment images. *Frontiers in Neuroscience*, *16*, 1084118.

Gozzi, F., Bertolini, M., Gentile, P., Verzellesi, L., Trojani, V., De Simone, L., ... & Cimino, L. (2023). Artificial Intelligence-Assisted Processing of Anterior Segment OCT Images in the Diagnosis of Vitreoretinal Lymphoma. *Diagnostics*, *13*(14), 2451.

Hasan, N., Driban, M., Mohammed, A. R., Schwarz, S., Yoosuf, S., Barthelmes, D., ... & Chhablani, J. (2023). Effects of hydroxychloroquine therapy on choroidal volume and choroidal vascularity index. *Eye*, 1-5.

Healy, S., McMahon, J., Owens, P., Dockery, P., & FitzGerald, U. (2018). Threshold-based segmentation of fluorescent and chromogenic images of microglia, astrocytes and oligodendrocytes in FIJI. *Journal of Neuroscience Methods*, *295*, 87-103.

Huang, D., Swanson, E. A., Lin, C. P., Schuman, J. S., Stinson, W. G., Chang, W., ... & Fujimoto, J. G. (1991). Optical coherence tomography. *Science*, *254*(5035), 1178-1181.

Huang, X., Lee, S. J., Kim, C. Z., & Choi, S. H. (2022). An improved strabismus screening method with combination of meta-learning and image processing under data scarcity. *PLoS One*, *17*(8), e0269365.

Kashani, A. H., Chen, C. L., Gahm, J. K., Zheng, F., Richter, G. M., Rosenfeld, P. J., ... & Wang, R. K. (2017). Optical coherence tomography angiography: a comprehensive review of current methods and clinical applications. *Progress in Retinal and Eye Research*, *60*, 66-100.

Kim, M., Ha, M. J., Choi, S. Y., & Park, Y. H. (2018). Choroidal vascularity index in type-2 diabetes analyzed by swept-source optical coherence tomography. *Scientific Reports*, *8*(1), 70.

Landini, G., Randell, D. A., Fouad, S., & Galton, A. (2017). Automatic thresholding from the gradients of region boundaries. *Journal of Microscopy*, *265*(2), 185-195.

Leitgeb, R., Hitzenberger, C., & Fercher, A. (2003). Performance of fourier domain vs. time domain optical coherence tomography. *Optics Express*, *11*(8), 889-894.

Manjunath, V., Taha, M., Fujimoto, J. G., & Duker, J. S. (2010). Choroidal thickness in normal eyes measured using Cirrus HD optical coherence tomography. *American Journal of Ophthalmology*, *150*(3), 325-329.e321.

Mohamed Razali, M. R., Ismail, W., Ahmad, N. S., Bahari, M., Mohd Zaki, Z., & Radman, A. (2017). An adaptive thresholding method for segmenting dental X-ray images. *Journal of Telecommunication, Electronic and Computer Engineering (JTEC)*, *9*(4), 1-5.

Nassif, N. A., Cense, B., Park, B. H., Pierce, M. C., Yun, S. H., Bouma, B. E., ... & De Boer, J. F. (2004). In vivo high-resolution video-rate spectral-domain optical coherence tomography of the human retina and optic nerve. *Optics Express*, *12*(3), 367-376.

Niblack, W. (1986). *An introduction to digital image processing*, Prentice Hall, 1-215.

Nichele, L., Persichetti, V., Lucidi, M., & Cincotti, G. (2020). Quantitative evaluation of ImageJ thresholding algorithms for microbial cell counting. *OSA Continuum*, *3*(6), 1417-1427.

Patton, N., Aslam, T. M., MacGillivray, T., Deary, I. J., Dhillon, B., Eikelboom, R. H., Yogesan, K., & Constable, I. J. (2006). Retinal image analysis: Concepts, applications and potential. *Progress in Retinal and Eye Research*, *25*(1), 99-127.

Qi, Z., Liu, X., Xiong, S., Wang, J., Chen, J., Zhu, Z., ... & Xu, X. (2023). Macular and peripapillary Choroidal Vascularity Index in children with different refractive status. *Eye*, 1-8.

Qiu, B., Huang, Z., Liu, X., Meng, X., You, Y., Liu, G., ... & Lu, Y. (2020). Noise reduction in optical coherence tomography images using a deep neural network with perceptually-sensitive loss function. *Biomedical Optics Express*, *11*(2), 817-830.

Quiroz-Reyes, M. A., Quiroz-Gonzalez, E. A., Quiroz-Gonzalez, M. A., & Lima-Gomez, V. (2023). Postoperative choroidal vascular biomarkers in eyes with rhegmatogenous retinal detachment-related giant retinal tears. *International Journal of Retina and Vitreous*, *9*(1), 45.

Ratra, D., Tan, R., Jaishankar, D., Khandelwal, N., Gupta, A., Chhablani, J., & Agrawal, R. (2018). Choroidal structural changes and vascularity index in Stargardt disease on swept source optical coherence tomography. *Retina*, *38*(12), 2395-2400.

Sauvola, J., & Pietikäinen, M. (2000). Adaptive document image binarization. *Pattern Recognition*, *33*(2), 225-236.

Schindelin, J., Arganda-Carreras, I., Frise, E., Kaynig, V., Longair, M., Pietzsch, T., ... & Cardona, A. (2012). Fiji: an open-source platform for biological-image analysis. *Nature Methods*, *9*(7), 676-682.

Schneider, C. A., Rasband, W. S., & Eliceiri, K. W. (2012). NIH Image to ImageJ: 25 years of image analysis. *Nature Methods*, *9*, 671-675.

Singh, B. M., & Mridula. (2014). Efficient binarization technique for severely degraded document images. *CSI Transactions on ICT*, *2*(3), 153-161.

Sonoda, S., Sakamoto, T., Yamashita, T., Shirasawa, M., Uchino, E., Terasaki, H., & Tomita, M. (2014). Choroidal structure in normal eyes and after photodynamic therapy determined by binarization of optical coherence tomographic images. *Investigative Ophthalmology & Visual Science*, *55*(6), 3893-3899.

Spaide, R. F., Koizumi, H., & Pozzoni, M. C. (2008). Enhanced depth imaging spectral-domain optical coherence tomography. *American Journal of Ophthalmology*, *146*(4), 496-500.

Sull, A. C., Vuong, L. N., Price, L. L., Srinivasan, V. J., Gorczynska, I., Fujimoto, J. G., Schuman, J. S., & Duker, J. S. (2010). Comparison of spectral/Fourier domain optical coherence tomography instruments for assessment of normal macular thickness. *Retina*, *30*(2), 235-245.

Wang, D., Xiao, H., Lin, S., Fang, L., Gan, Y., Zhang, Y., ... & Zuo, C. (2023). Comparison of the choroid in primary open-angle and angle-closure glaucoma using optical coherence tomography. *Journal of Glaucoma*, 10-1097.

Cite as: Inam, O. (2023). Comparison of the effects of different local thresholding techniques on noise: A potential for optical coherence tomography image binarization. *Front Life Sci RT*, *4*(3), 138-144.